



Modelling and optimization of lead adsorption by $\text{CoFe}_2\text{O}_4\text{@CMC@HZSM-5}$ from aqueous solution using response surface methodology

Alireza Nasiri^a, Mohammad Malakootian^{b,c}, Neda Javid^{d,e,*}

^aEnvironmental Health Engineering Research Center, Kerman University of Medical Sciences, Kerman, Iran, email: nasiri_a62@yahoo.com/ARNasiri@Kmu.ac.ir

^bEnvironmental Health Engineering Research Center, Kerman University of Medical Sciences, Kerman, Iran, email: m.malakootian@yahoo.com

^cDepartment of Environmental Health, School of Public Health, Kerman University of Medical Sciences, Kerman, Iran

^dEnvironmental Health Engineering Research Center, Kerman University of Medical Sciences, Kerman, Iran, email: n.javid1367@gmail.com

^eDepartment of Environmental Health Engineering, Zarand School of Nursing, Kerman University of Medical Sciences, Kerman, Iran, email: n.javid1367@gmail.com

Received 17 August 2020; Accepted 12 December 2021

ABSTRACT

A modified magnetic nano-biocomposite based on zeolite ($\text{CoFe}_2\text{O}_4\text{@CMC@HZSM-5}$) was synthesized and characterized by X-ray diffraction, Fourier-transform infrared spectroscopy, field-emission scanning electron microscopy, vibrating sample magnetometer, and Brunauer–Emmett–Teller tests. $\text{CoFe}_2\text{O}_4\text{@CMC@HZSM-5}$ was applied as an adsorbent for the efficient removal of Pb(II). Then, the applicability of the nano-biocomposite adsorbent was investigated for the lead removal. To determine the relationship between effective parameters on lead adsorption, the response surface methodology was applied. Maximum removal efficiency by $\text{CoFe}_2\text{O}_4\text{@CMC@HZSM-5}$ under optimal conditions with a contact time of 300 min, pH = 5, Pb(II) concentration of 400 mg/L, and 0.4 g of the adsorbent (reactor volume = 200 mL) was 96% for synthetic and 75% for real samples, respectively. The adsorption of Pb(II) by $\text{CoFe}_2\text{O}_4\text{@CMC@HZSM-5}$ followed the Langmuir isotherm and pseudo-second-order kinetic models. According to the negative ΔH° values, the adsorption of Pb(II) onto $\text{CoFe}_2\text{O}_4\text{@CMC@HZSM-5}$ was exothermic and thermodynamics studies indicated that was not possible and spontaneous in nature. The magnetic nano-biocomposite adsorbent had good reusability and attained a high removal efficiency of 91% for Pb(II) after six consecutive adsorption cycles, thus can be recommended as a coefficient adsorbent for the removal of Pb(II) from contaminated water.

Keywords: Organometallic adsorbent; Pb(II); Magnetic nanocomposite; Bio-adsorbent; Response surface methodology

1. Introduction

Water pollution is a serious environmental problem and receives growing attention due to the deficiency of clean water [1–4]. Because of the rapid industrialization, the ecosystem and living organisms are at the risk of

heavy metal pollution [5]. Water polluted by heavy metals has received considerable attention since these metals are non-biodegradable, poisonous and carcinogenic, and can accumulate in living systems [6].

Aqueous lead is a major pollutant found all over world and can releases into the environment, particularly into

* Corresponding author.

water resources, because of anthropogenic actions [1,7]. Lead contamination is the result of various industrial activities, like lead batteries, phosphate fertilizers, electronics, wood vehicle emissions, painting, plating, textile, petroleum, and petrochemical industries, and has become a global concern in the last few decades [5,8]. The concentration of lead in natural water is 0.4–0.8 mg/L. This amount in the raw surface and underground water is 0.04–0.008 mg/L with an average of 0.01 mg/L [9,10]. Based on the World Health Organization, at a concentration of $>70 \mu\text{g/dL}$, lead (Pb(II)) is harmful for the central nervous system, basic cellular processes, liver, reproductive system, kidneys, and brain performance [6,11].

Various technologies to remove pollutants from contaminated wastewater, including chemical precipitations, ion exchange, and advanced oxidation processes [12–20], membrane filtration, electrolysis or reverse osmosis techniques, have been suggested and studied. Some disadvantages of removal methods include incomplete processing, high cost, production of toxic sludge (physical and chemical methods), clogging pores and wastewater ponding (filtration) [21]. The adsorption process is a priority because of its lower initial cost, simplicity of operation, lack of harmful secondary production, low sensitivity to stream fluctuations, the ineffectiveness of toxic chemicals in the process, removal of most organic pollutants [16,19,22–28], and cost-effectiveness [4,23,29,30].

Zeolite is defined as crystalline aluminium silicate produced through shared oxygen atoms in an aluminum framework and silicate tetrahedral in different pore sizes. Among different adsorbents, zeolite is promising for metal purification and has an efficiency as high as that of adsorbents in gas purification, ion exchangers, petroleum refinement catalysis, and petrochemistry because of its elevated cation exchange capacity (CEC) [31–33]. Zeolite has been applied in its primary form and corrected form using different chemical reagents, like surfactants, organic compounds, and inorganic substances. The modification process can be performed in single steps such as cation exchange or multiple steps such as cation exchange, oxidization, and reduction [34–38]. One of the major problems in the use of nanometer and micrometer powder adsorbents is their separation from the environment after synthesis and the completing the adsorption process. Adsorbent separation from the reaction medium challenge by time-consuming methods such as filtration and centrifugation will be eliminated by magnetization. Synthesis and use of magnetic composites can be the solution to this problem; after the ion exchange process, the adsorbent can be isolated from the adsorption environment easily and rapidly by using a permanent or electric magnet [39,40].

Various adsorbents such as Ni/ZnO-HZSM-5 [2], Ru/hierarchical HZSM-5 [1], alkali-modified HZSM-5, PVA/zeolite nanofibers [41], magnetic zeolite [42], iron oxide-coated zeolite [43], zeolite/aluminum composite [44], manganese oxide-coated zeolite [45], magnetic zeolites [46], Cu(I)-Y-zeolite [47], versatile magnetic gel from peach gum polysaccharide, indian saffron – turmeric (*Curcuma longa*) embedded supermacroporous cryogel discs and other adsorbents have been incorporated to remove heavy metals from aqueous media [48–55].

Because of the availability, cost-effectiveness, renewability, and stable nature of cellulose, different eco-friendly cellulose-oriented materials have been provided and applied as sorbents or photocatalysts to remove aqueous pollutants [56–61]. Nonetheless, using raw cellulose because of its lower surface area, poor interaction with pollutants, lower solubility, and reusability is restricted. Accordingly, ether, ester, ionic functionalization, and cellulose combined with nanomaterials can offer advanced cellulose derivatives [62–64]. Carboxymethyl cellulose (CMC) is essential to improve the structural features of $\text{CoFe}_2\text{O}_4@\text{CMC}@\text{HZSM-5}$ nano adsorbent. Due to the presence of CMC in the structure of $\text{CoFe}_2\text{O}_4@\text{CMC}@\text{HZSM-5}$ nano-biomagnetic composite, resulting in the larger surface area of adsorbent. Also, carboxyl and hydroxyl groups in CMC induce the electrostatic attraction between Pb and $\text{CoFe}_2\text{O}_4@\text{CMC}@\text{HZSM-5}$ nano-biomagnetic composite surface. Therefore, several molecules of Pb are located in near the adsorbent surface [65].

Based on the literature, $\text{CoFe}_2\text{O}_4@\text{CMC}@\text{HZSM-5}$ has not been utilized as a magnetic nanoadsorbent yet. Thus, in this study, compositing zeolite with cobalt ferrite increased the adsorbent adsorption ability, and adsorbent separation from the environment was eliminated by magnetization. This study aimed at preparing magnetically separable $\text{CoFe}_2\text{O}_4@\text{CMC}@\text{HZSM-5}$ as a nano-adsorbent for removing lead from aqueous solutions. Also, we investigated effective factors, including solution pH, adsorbent dose, primary concentrations, and contact length. The synthesized adsorbent had an enhanced capacity to remove Pb(II).

2. Experimental procedure

2.1. Materials and solutions

All chemical materials, including $\text{Pb}(\text{NO}_3)_2$, HCl, NaOH, $\text{FeCl}_3 \cdot 6\text{H}_2\text{O}$, and $\text{CoCl}_2 \cdot 6\text{H}_2\text{O}$ were analytical-grade reagents purchased by Merck (Germany). Artificial zeolite (HZSM-5) with a 5.5 Å pore size and mole ratio of $\text{SiO}_2/\text{Al}_2\text{O}_3 = 80$ was purchased from Iran Zeolite Company (Tehran, Iran). The water used for preparing all solutions was obtained from a deionized water system. The solutions' pH was set with sodium hydroxide or hydrochloric acid solution.

2.2. Analytical methods

The solutions' pH was assessed via a pH meter (model: WTW). A magnetic stirrer (model: Shimi Tajhiz) was employed for stirring, and scales (model: Shimadzu-Libror) were used for weighing. The Pb concentration in solutions was assessed with flame atomic absorption spectroscopy (FAAS) (model: Varian Spectra A 220, Australia) with an air-acetylene flame ($\lambda = 240.7 \text{ nm}$) [5].

2.3. Preparation of $\text{CoFe}_2\text{O}_4@\text{CMC}@\text{HZSM-5}$

The magnetic nanocomposite was prepared using salts of iron chloride $\text{FeCl}_3 \cdot 6\text{H}_2\text{O}$, cobalt chloride $\text{CoCl}_2 \cdot 6\text{H}_2\text{O}$, CMC and HZSM-5 zeolite. First, salts of iron chloride $\text{FeCl}_3 \cdot 6\text{H}_2\text{O}$ and cobalt chloride $\text{CoCl}_2 \cdot 6\text{H}_2\text{O}$ (2:1) were dissolved in 100 mL of distilled water (DW) followed by 1 g

of CMC and finally 1 g of HZSM-5 zeolite were added to the solution. Subsequently, NaOH was added to the resulting suspension for 1 h until the solution pH reached 13. The reaction container's color changed and became black after 1 h of stirring. Then, the reaction container was transferred to the microwave and was irradiated by microwave waves. The radiation process was performed in three periods of 5 min with 50% power of the microwave and 30 s with the off mode. The product was a light and black powder that was subjected to washing many times using DW and dried in the oven (100°C within 24 h) (Fig. 1).

2.4. Characterization techniques of $\text{CoFe}_2\text{O}_4\text{@CMC@HZSM-5}$

To measure the porosity of the surface area adsorbents, the Brunauer–Emmett–Teller (BET) method using a Micrometrics Model 021LN2 transfer device was employed. Fourier-transform infrared spectroscopy (FT-IR) using a WQF-510 FT-IR Spectrometer was used to determine the adsorbent's functional group. To determine the presence of the crystalline structure of cobalt ferrite in the adsorbent, X-ray diffraction (XRD) with a Philips X-Pert device (the Netherlands) was employed. Characterization of the specimens was done using a field-emission scanning electron microscopy (FE-SEM) (200 Nova Nano SEM, FEI Co.). The magnetic properties of the $\text{CoFe}_2\text{O}_4\text{@CMC@HZSM-5}$ were characterized by vibrating sample magnetometer (VSM) (Lake Shore Cryotronics-7404) at room temperature.

2.5. pH point of zero charge (pH_{PZC}) measurements

For determination of the pH point of zero charges (pH_{PZC}) of the $\text{CoFe}_2\text{O}_4\text{@CMC@HZSM-5}$ was used solid addition method. 100 mL of KCl solution (0.1 M) was prepared at 10 different pH (2–11) values. 0.01 g of $\text{CoFe}_2\text{O}_4\text{@}$

$\text{CoFe}_2\text{O}_4\text{@CMC@HZSM-5}$ was added to each solution. The prepared solutions were kept at room temperature (24 h). The pH initial (pH_i) and final pH (pH_f) values of the solutions were evaluated by pH meter. ΔpH ($\text{pH}_f - \text{pH}_i$) and pH_f the chart was drawn for determination of the pH_{PZC} . The intersection point of $\Delta\text{pH} = 0$ was taken as pH_{ZPC} . The pH of solutions was adjusted by NaOH and HCL 0.1 N [65].

2.6. Batch sorption studies for lead removal

The experiments were performed at the Environmental Health Engineering Research Center of Kerman University of Medical Sciences (Iran). This study with reactor volume = 200 mL examined the parameters affecting removal efficiency, including pH (1–9), contact duration (30–360 min), primary Pb(II) level (50–800 mg/L), and adsorbent dosage (0.01–0.4 g). Stock heavy metal solution (1,000 mg/L) was provided through dissolving $\text{Pb}(\text{NO}_3)_2$ in 100 mL of deionized water, and then other solutions were prepared with the intended concentrations. After adding the required amount of adsorbent to each sample, the adsorbent and heavy metals were thoroughly mixed using a magnetic stirrer (300 rpm). Batch experiments were conducted in flasks with a volume of 100 mL at 25°C in triplicate.

The adsorbent was separated from the reaction medium with an external magnet. The Pb^{2+} level in solutions was calculated by an atomic absorption spectrometer ($\lambda = 240.7 \text{ nm}$) [6]. The adsorption capacity adsorbent (analyte sorbed level by the sorbent) (Q_e , mg/g) and the percentage of removal efficiency were determined by two following formulas:

$$Q_e = \frac{[(C_0 - C_e) V]}{m} \quad (1)$$

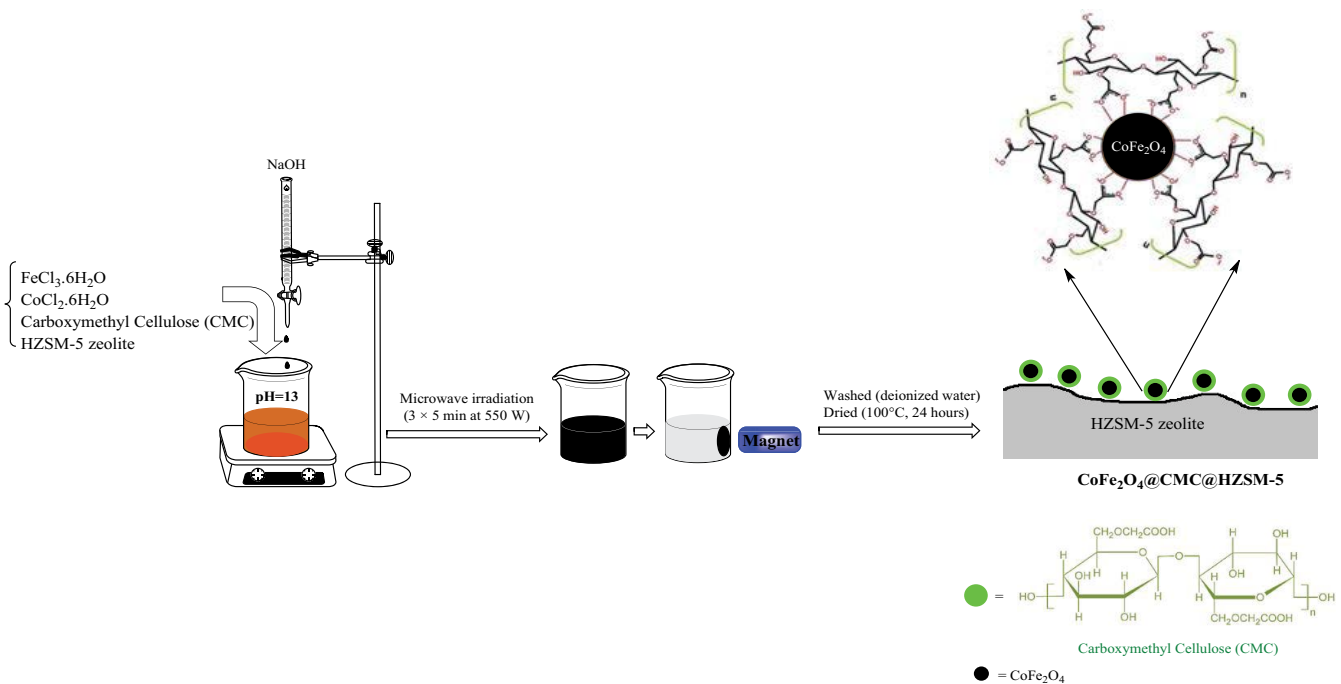


Fig. 1. Schematic representation of $\text{CoFe}_2\text{O}_4\text{@CMC@HZSM-5}$ synthesis.

$$R = \left[\frac{(C_0 - C_e)}{C_0} \right] \times 100 \quad (2)$$

where Q_e is the adsorption capacity of $\text{CoFe}_2\text{O}_4\text{@CMC@HZSM-5}$ in mg/g, C_0 indicates the primary level in mg/L, C_e represents the equilibrium level of metal ions in mg/L, V refers to the metal ion solution volume (L), and m represents the amount of adsorbent (g) [18].

2.7. Adsorption isotherms

Analysis of the equilibrium values was done using two adsorption isotherms: Langmuir and Freundlich. The former supposes that the adsorption process in monolayer is done on the adsorbent characterized by a homogenous surface with binding sites with the similar affinity for the adsorption, however, no interaction is observed between adsorbates. The latter supposes that the adsorption is done on the heterogeneous surface, where there is an interaction between adsorbed molecules and the adsorbed ion content rises sharply with an increase in the primary content [7]. The linear types of Langmuir and Freundlich models are demonstrated in Eqs. (3) and (4), respectively.

$$\frac{C_e}{q_e} = \left(\frac{1}{Q^\circ b} \right) + \left(\frac{C_e}{Q^\circ} \right) \quad (3)$$

$$\log(q_e) = \log(K_F) + \left(\frac{1}{n} \right) \log C_e \quad (4)$$

q_e (mg/g) represents adsorption capacity and C_e (mg/L) indicates equilibrium concentration; Q° (mg/g) shows the highest adsorption capability related to Pb^{2+} on the surface of $\text{CoFe}_2\text{O}_4\text{@CMC@HZSM-5}$; b (L/mg) represents the rate of adsorption (Langmuir constant); K_F and n represent Freundlich constants; K_F indicates adsorption ability (mg/g)(L/mg) $1/n$; and n shows the tendency to adsorb [66].

2.8. Adsorption kinetics and thermodynamics

Kinetic investigations present crucial data on the adsorption mechanism. For determining this mechanism, Pb(II) ions adsorption was evaluated as a function of time. Pseudo-first- as well as pseudo-second-order models were adopted for determining the adsorption kinetics. The linear types of pseudo-first- and pseudo-second-order models are given in Eqs. (5) and (6), respectively.

$$\log(q_e - q_t) = \log q_e - \left(\frac{k_1 t}{2.303} \right) \quad (5)$$

$$\frac{t}{q_t} = \left(\frac{1}{k_2 q_e^2} \right) + \left(\frac{t}{q_e} \right) \quad (6)$$

where q_e (mg/g) represents adsorption capacity, q_t represents Pb(II) capacity adsorbed on the $\text{CoFe}_2\text{O}_4\text{@CMC@HZSM-5}$ surface at time t (mg/g), k_1 and k_2 indicate the

constants of the equilibrium rate of first- and second-order kinetics, respectively (1/h), and t represents the adsorption time (h) [6].

To determine the temperature impact on the Pb(II) sorption behaviors by $\text{CoFe}_2\text{O}_4\text{@CMC@HZSM-5}$, Eqs. (7)–(9) were applied for calculating the intrinsic thermodynamic factors associated with the sorption process, like an alteration in Gibbs free energy (ΔG°), enthalpy (ΔH°), and entropy (ΔS°) [Eqs. (7)–(9)].

$$\ln K_c = \frac{\Delta S^\circ}{R} - \frac{\Delta H^\circ}{RT} \quad (7)$$

$$\Delta G^\circ = -RT \ln K_c \quad (8)$$

$$K_c = m \frac{q_e}{C_e} \quad (9)$$

where R indicates the gas constant (8.314 (J/mol K)), T denotes temperature (K), m represents the adsorbent dose (g/L), and K_c is the equilibrium constant.

2.9. Design of experiments

Response surface methodology was applied for estimating all variables effect on the Pb(II) removal using $\text{CoFe}_2\text{O}_4\text{@CMC@HZSM-5}$. The model benefits from the mathematical and statistical methods [6,60]. Data analysis was performed using Minitab 19 and Excel 2016. To prevent systemic errors, experiments were conducted in random order with three replicates [23].

2.10. Real solution

The adsorption test was carried out with synthetic solutions. Following determination of optimal conditions, the experiments were performed on wastewater from the wastewater steel industry for evaluating the interventions effect in a real sample.

3. Results and discussion

3.1. Characterizing the $\text{CoFe}_2\text{O}_4\text{@CMC@HZSM-5}$

3.1.1. FT-IR spectroscopy

Comparative FT-IR of CMC, HZSM-5, and $\text{CoFe}_2\text{O}_4\text{@CMC@HZSM-5}$ are demonstrated in Fig. 2. In the FT-IR spectrum of carboxymethyl cellulose the wide absorption band at 3424 cm^{-1} belonged to the stretching vibrations of the OH groups. The absorption band at 2920 cm^{-1} belonged to the stretching vibrations of the CH_2 groups. The typical vibration of CMC was at 1111 and 1160 cm^{-1} , representing the stretching vibration of the C–OH groups. The strong broad band at 3444 cm^{-1} corresponded to the stretching vibrations of the intra molecular hydrogen bond. The band at 2920 cm^{-1} showed the stretching vibrations of the C–H bonds. Moreover, the strong peak at 1648 cm^{-1} was associated with the stretching vibrations of the carboxyl group, and the absorption bands in the range 1100 to 1150 cm^{-1} belong to C–O stretching vibrations in

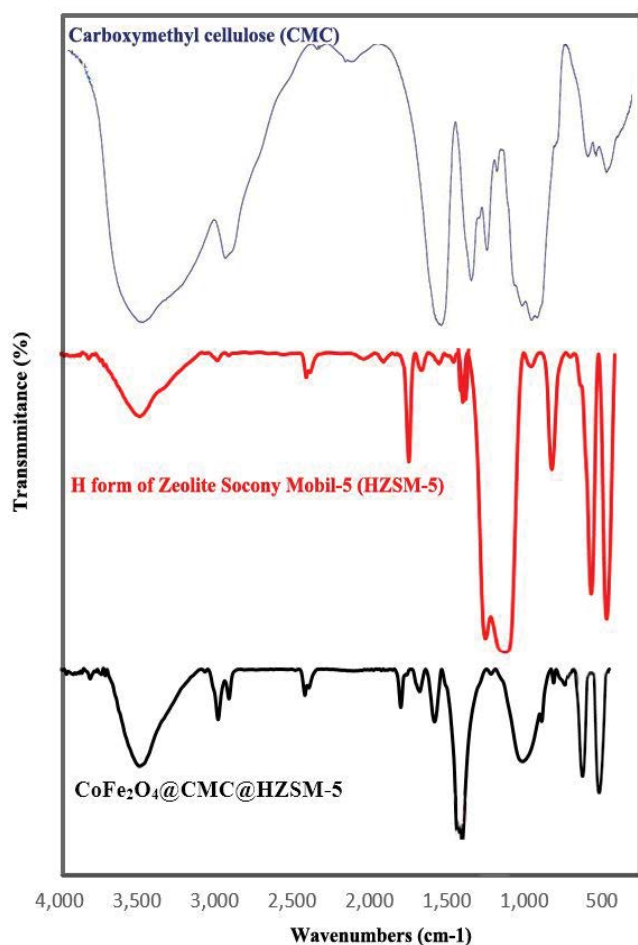


Fig. 2. The FT-IR spectrum of CMC, HZSM-5, and CoFe_2O_4 @CMC@HZSM-5 magnetic nanocomposite.

carboxymethyl cellulose. In the FT-IR spectrum of HZSM-5 the wide absorption band at $3,424\text{ cm}^{-1}$ belonged to the stretching vibrations of the OH groups. The absorption bands at $1,102\text{ cm}^{-1}$ (internal asymmetric stretch), 799 cm^{-1} (external symmetric stretch), 548 cm^{-1} (double ring vibration) and 450 cm^{-1} (T-O bending vibration of the Si-O and Al-O internal tetrahedral) were attributed to the typical characteristics of HZSM-5. In addition, an asymmetric stretch vibration of the band at $1,221\text{ cm}^{-1}$ was a strong evidence for HZSM-5 zeolite [30]. Meanwhile, this band can demonstrate the absence of amorphous silica and even can be used to determine the crystallinity of HZSM-5 zeolites [37,38]. In the FT-IR of CoFe_2O_4 @CMC@HZSM-5, the wide absorption band at $3,431\text{ cm}^{-1}$ was associated with the stretching vibrations of hydroxyl groups that overlaid with acidic OH group of carboxyl group. The absorption band at $1,623\text{ cm}^{-1}$ belonged to the stretching vibrations of the carboxyl group, confirming the presence of carboxymethyl cellulose in the structure of CoFe_2O_4 @CMC@HZSM-5. Also, Strong absorption bonds at $1,349$ and $1,381\text{ cm}^{-1}$ indicates the presence of HZSM-5 zeolite in the structure of CoFe_2O_4 @CMC@HZSM-5. In addition, the absorption bands around $400\text{--}600\text{ cm}^{-1}$ in CoFe_2O_4 @CMC@HZSM-5 is related to vibrations of metal-oxygen groups (Co-O, Fe-O) in the cobalt ferrite and zeolite structure (Si-O, Al-O).

3.1.2. FE-SEM and energy-dispersive X-ray spectroscopy of CoFe_2O_4 @CMC@HZSM-5

The surface morphology of the adsorption material was assessed by FE-SEM. Morphological results of magnetic nanocomposites CoFe_2O_4 @CMC@HZSM-5 are illustrated in Fig. 3. The attendance of CMC in the CoFe_2O_4 @CMC@HZSM-5 structure causes form the smoothly, uniformly, and loosely aggregated sphere-shaped of magnetic nanocomposites. Based on the particles size, it can be understood

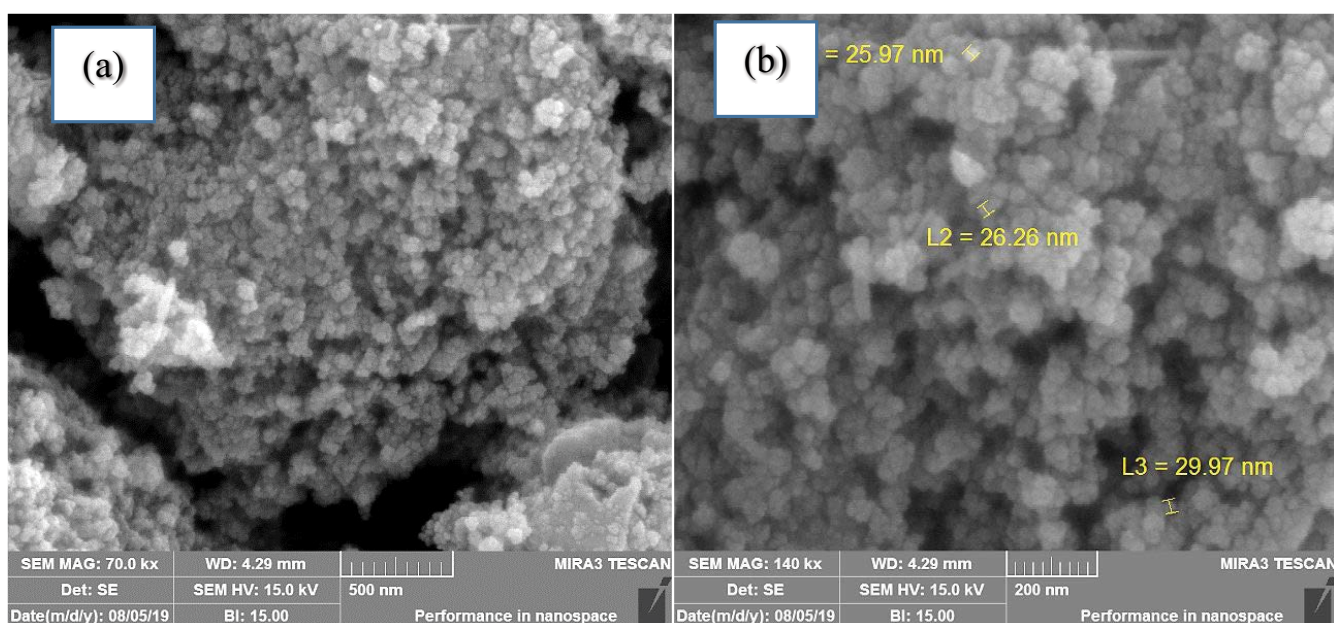


Fig. 3. The FE-SEM images of magnetic nanocomposite CoFe_2O_4 @CMC@HZSM-5 (a and b).

that the average particles size of $\text{CoFe}_2\text{O}_4\text{@CMC@HZSM-5}$ are about 27 nm.

The synthesized $\text{CoFe}_2\text{O}_4\text{@CMC@HZSM-5}$ magnetic nanoadsorbent purity and chemical structure were evaluated by energy-dispersive X-ray spectroscopy (EDS) analysis (Fig. 4). The results demonstrate 46.44% O, 26.82% Fe, 14.16% Co, 8.56% C, 3.88% Si, and 0.15% Al in the chemical structure of $\text{CoFe}_2\text{O}_4\text{@CMC@HZSM-5}$ magnetic nanoadsorbent which are following the expected values.

3.1.3. XRD of $\text{CoFe}_2\text{O}_4\text{@CMC@HZSM-5}$

The XRD patterns were prepared separately from CMC, HZSM-5, CoFe_2O_4 , and $\text{CoFe}_2\text{O}_4\text{@CMC@HZSM-5}$ and were compared with each other (Fig. 5). In the CMC XRD pattern, the index peak can be seen in the area of 18.28° , 23.15° and 24.06° peaks are belong to HZSM-5 and the values which are seen in $2\theta = 30.26^\circ$, 35.70° , 43.35° , 53.74° , 57.29° , and 62.81° are related to cobalt ferrite. The XRD results of $\text{CoFe}_2\text{O}_4\text{@CMC@HZSM-5}$ magnetic nanocomposite in the range from 10° to 80° ($2\theta = 10^\circ\text{--}80^\circ$) are depicted in Fig. 5. The sharp diffractions in regions 18.28° , 23.15° , 24.06° , 30.26° , 35.70° , 43.35° , 53.74° , 57.29° , and 62.81° indicated the crystalline structure in the spinel shape, which was consistent with the Joint Committee on Powder Diffraction Standards (no. 96-900-5813). The presence of sharp and strong peaks in this pattern and comparison of peak locations with reference data indicated the crystalline structure of cobalt ferrite with complete crystallization that has preserved the crystalline structure of $\text{CoFe}_2\text{O}_4\text{@CMC@HZSM-5}$, after being composite with carboxymethylcellulose and zeolite. An average value of $\text{CoFe}_2\text{O}_4\text{@CMC@HZSM-5}$ crystallite size of 8.67 nm as calculated by XRD. According to the literature the crystallinity and crystallite size of the adsorbent are important features which could affect the reactive performance and the removal mechanism [69–70].

3.1.4. Vibrating sample magnetometer

The results of VSM analysis of magnetic nanocomposite $\text{CoFe}_2\text{O}_4\text{@CMC@HZSM-5}$ are demonstrated in Fig. 6. Magnetic coercive force (H_c), saturation magnetization (M_s), and remnant magnetization (M_r) are equal to 0.73 Oe, 41.36 emu/g, and 50 emu/g, in that order. The results revealed that the magnetic nanocomposite $\text{CoFe}_2\text{O}_4\text{@CMC@HZSM-5}$ had a ferromagnetic effect with elevated saturation magnetization and high magnetic coercive force. It could be quickly separated and retrieved from the reaction container using a magnet and could be reused in subsequent periods.

3.1.5. Brunauer–Emmett–Teller

Information obtained from the BET test showed that surface area, pore volume, and pore size equaled $235.2181\text{ m}^2/\text{g}$, $0.207319\text{ cm}^3/\text{g}$, and 3.52 nm , respectively. The results of BET analysis of magnetic nanocomposite $\text{CoFe}_2\text{O}_4\text{@CMC@HZSM-5}$ are given in Table 1.

3.2. Effect of pH solution on removal efficiency

pH is a major parameter influencing the surface charge of solid adsorbents, as well as the forming metal hydroxide [5]. The pH effect on the Pb(II) removal using $\text{CoFe}_2\text{O}_4\text{@CMC@HZSM-5}$ was investigated at pH 1–9 and different Pb(II) initial concentrations of 50 to 800 mg/L. The findings are dividable into two pH regions. In the first pH region (1–5), the adsorption efficiency quickly increased following an increase in pH. $\text{CoFe}_2\text{O}_4\text{@CMC@HZSM-5}$ indicated a highest removal of 96% at pH 5. Fig. 7 shows the pH tests results, the interaction between two variables (pH and time), and their impact on Pb(II) removal efficiency from aqueous solutions.

The Pb(II) removal efficiency elevated from 5% to 96% after an increase in pH from 1 to 5. In the second pH

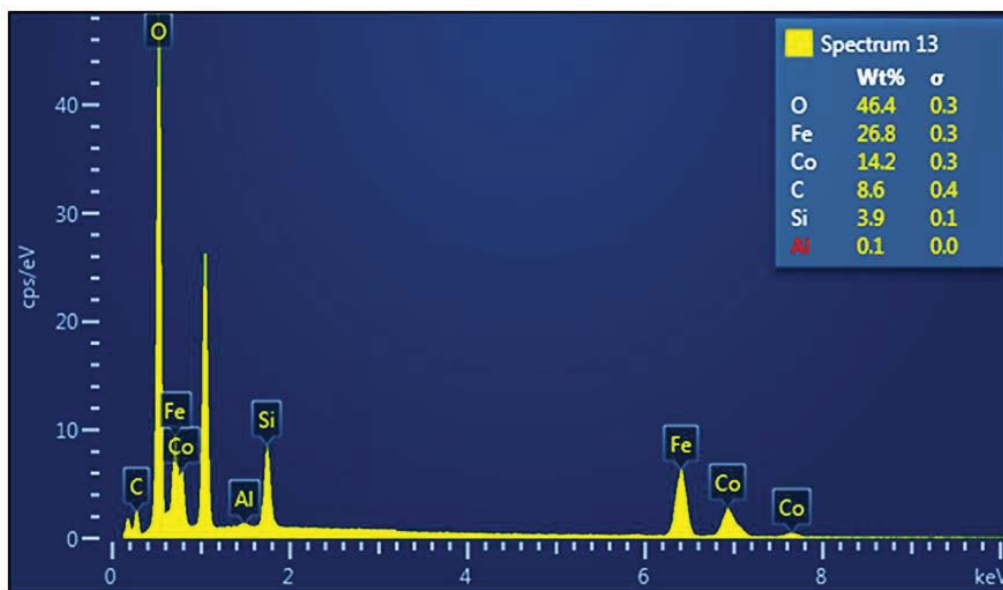


Fig. 4. The EDS of $\text{CoFe}_2\text{O}_4\text{@CMC@HZSM-5}$ magnetic nanoadsorbent.

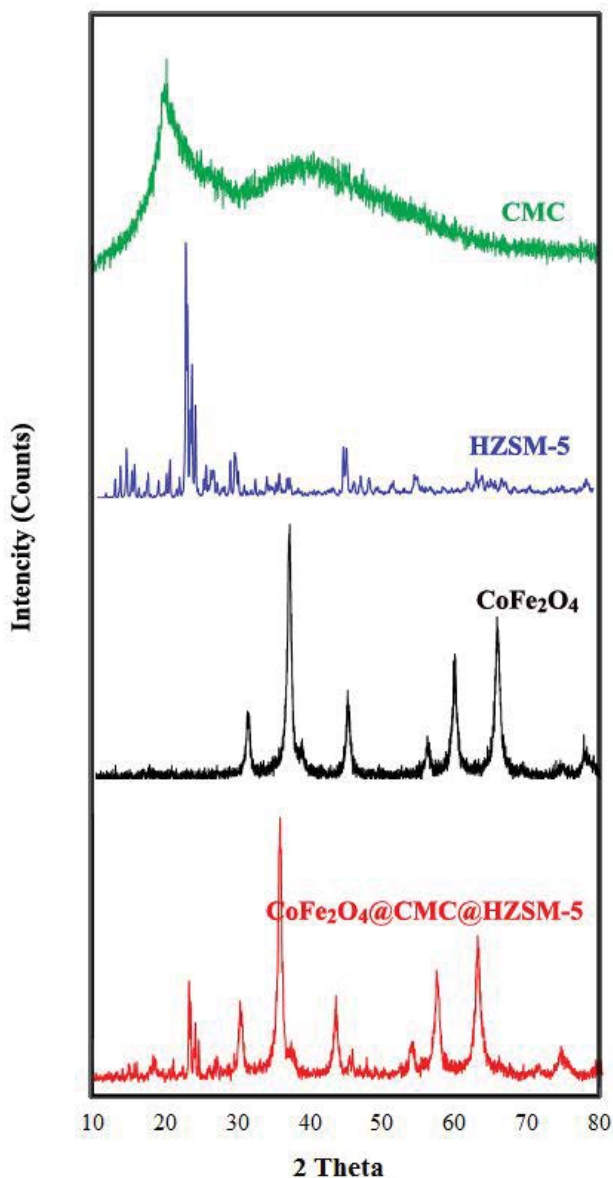


Fig. 5. The XRD patterns of CMC, HZSM-5, CoFe_2O_4 and $\text{CoFe}_2\text{O}_4@CMC@HZSM-5$ magnetic nanocomposite.

region (5 to 9), the adsorption efficiency kept nearly constant. The data achieved from pH for the study of Pb(II) ion can be described as follows: (1) the surface features of $\text{CoFe}_2\text{O}_4@CMC@HZSM-5$, and (2) the surveyed Pb(II) features in aqueous solution. In aqueous solutions, the magnetic surface is covered by FeOH groups [67]. The solution pH can influence the surface charge of $\text{CoFe}_2\text{O}_4@CMC@HZSM-5$, and this affects Pb(II) adsorption by the surface of $\text{CoFe}_2\text{O}_4@CMC@HZSM-5$. The cause of this event is related to the cationic structure of lead and pH_{ZPC} of $\text{CoFe}_2\text{O}_4@CMC@HZSM-5$. pH_{ZPC} is one of the parameters used in the adsorption process. pH_{ZPC} indicates the point at which the charge at the surface of the adsorbent is zero and at pHs higher than that, the adsorbent surface has a negative charge and below that the adsorbent surface has a positive charge. In this study, the pH of $\text{CoFe}_2\text{O}_4@$

Table 1

The results of BET analysis of magnetic nanocomposite $\text{CoFe}_2\text{O}_4@CMC@HZSM-5$

Entry	Parameter	Extent
1	BET surface area	235.2181 m^2/g
2	Pore volume	0.207319 cm^3/g
3	Pore size	3.52 nm

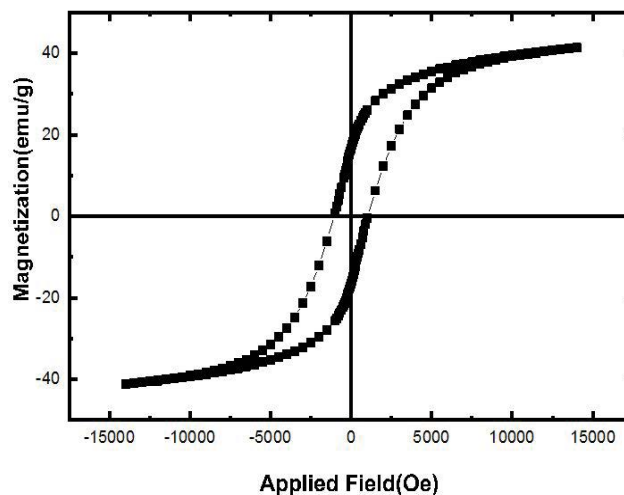


Fig. 6. Magnetic hysteresis curve of magnetic nanocomposite $\text{CoFe}_2\text{O}_4@CMC@HZSM-5$.

$\text{CoFe}_2\text{O}_4@CMC@HZSM-5$ was determined 3 ($\text{pH}_{ZPC} = 3$). The surface charge of $\text{CoFe}_2\text{O}_4@CMC@HZSM-5$ was negative at pH above 3 and the number of negative charges was increased with increasing pH. Increasing the solution pH reduces the positive charge and enhances the negative charge of the adsorbent surface, which increased the attraction force between the adsorbent and the Pb(II) [63]. At a low pH ($\text{pH} < 3$), surface functional groups of the magnetic zone and zeolite (adsorbent) have positive charges, making a strong repulsion force between them and Pb^{2+} . Our findings are in line with those of several investigations, including Uogintè et al. [6] and Venkateswarlu et al. [68].

3.3. Effect of primary Pb(II) level on removal efficiency

Investigating the impact of primary Pb(II) level on removal efficiency showed that with increasing lead concentration, removal efficiency enhanced. The results of the primary Pb(II) level effect, the interaction of the two variables (the amount of adsorbent and Pb(II) level), and their impacts on Pb(II) removal efficiency from aqueous solutions are displayed in Fig. 8.

By increasing lead level from 50 to 400 mg/L the removal efficiency was increased, but no remarkable change was observed after that, so that the maximum removal of lead was 96% at 400 mg/L concentration. In other words, according to Le Chatelier's principle, while using a disturbance or stress to a system in equilibrium, the equilibrium can move in such a way as to counteract the constraint effect.

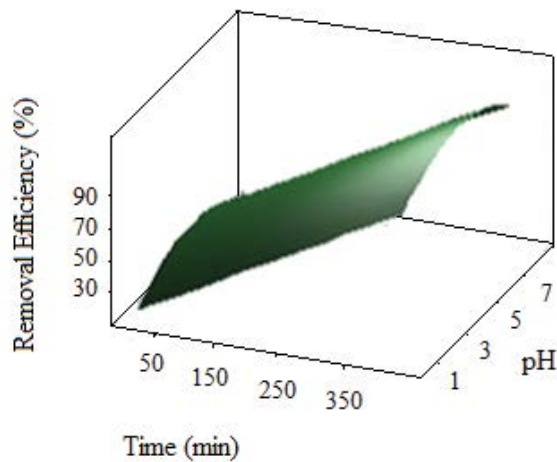


Fig. 7. Effect of pH, interaction of two variables (pH and time (min)) and their impact on removal efficiency of Pb(II) from aqueous solutions (Pb(II) concentration = 400 mg/L and amount of adsorbent = 0.4 g).

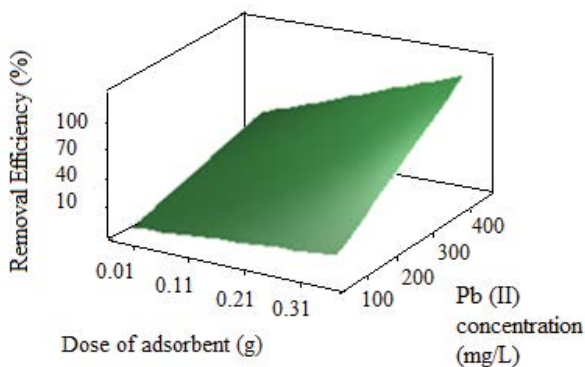


Fig. 8. Effect of initial Pb(II) concentration, interaction of two variables (initial Pb(II) concentration (mg/L) and the amount of adsorbent (g)), and their impact on removal efficiency of Pb(II) from aqueous solutions (contact time = 300 min and pH = 5).

Hence, by an increase in the Pb concentration, the equilibrium system decreases its concentration. With increasing lead level more than 400 mg/L due to the saturation of the exchange sites by adsorption, removal efficiency was decreased. The results of the effect of primary Pb(II) level on removal efficiency were in line with the of Shirzadi et al. [5] and Miranda et al. results [7].

3.4. Impact of contact time on removal efficiency

We examined the Pb(II) adsorption at different contact times. The contact time ranged from 30 to 360 min, and after the test, the Pb(II) level in the solution was assessed. According to the results, the removal efficiency was 96% after 300 min. Therefore, the optimum contact time was 5 h to remove Pb(II). Fig. 9 indicates the results of the contact time impact, the interaction of two variables (Pb(II) concentration and time), and their impact on removal efficiency of Pb(II) from aqueous solutions.

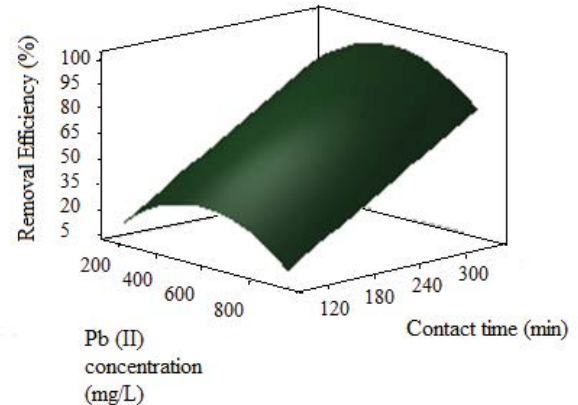


Fig. 9. Effect of contact time, interaction of two variables (Pb(II) concentration (mg/L) and contact time (min)), and their impact on removal efficiency of Pb(II) from aqueous solutions (pH = 5 and amount of adsorbent = 0.4 g).

Following increasing the contact time, the remaining Pb(II) level in the solution was reduced. The contact time to achieve equilibrium condition was 300 min and thereafter remained approximately stable due to the saturation of the consumed adsorbent [5]. The findings obtained by the contact time impact on removal efficiency was similar to the results of Shirzadi et al. [72] and Eljamal et al. [30].

3.5. Effect of the amount of adsorbent on removal efficiency

The Pb(II) removal efficiency was directly associated with changes in the amount of adsorbent by an increase in the amount of adsorbent from 0.01 to 0.4 g. Fig. 10 represents the findings obtained by the effects of adsorbent dose, interaction of two variables (the amount of adsorbent and pH), and their impact on Pb(II) removal efficiency from aqueous solutions.

The adsorbent level and removal efficiency are directly dependent on the Pb(II) removal from solutions with $\text{CoFe}_2\text{O}_4\text{@CMC@HZSM-5}$. With increasing the amount of adsorbent from 0.01 to 0.4 g, the removal efficiency was increased from 10% to 96% because of the increased adsorption surface active sites, and thereafter remained approximately stable. The reasons for this result are the increase in active surface sites and the increase in the encounter between the Pb(II) and $\text{CoFe}_2\text{O}_4\text{@CMC@HZSM-5}$. When the amount of adsorbent was increased, adsorption capacity (q_e) was decreased. These results are in line with the results of other studies, including Huang et al. [29] and Gaffer et al. [45].

3.6. Adsorption isotherm assessment

Adsorption isotherms were applied for estimating the level of lead ion adsorbed onto the $\text{CoFe}_2\text{O}_4\text{@CMC@HZSM-5}$. The Langmuir and Freundlich isotherm of Pb(II) using $\text{CoFe}_2\text{O}_4\text{@CMC@HZSM-5}$ are illustrated in Figs. 11a and b. Table 2 represents the equilibrium information obtained from Pb(II) adsorption by $\text{CoFe}_2\text{O}_4\text{@CMC@HZSM-5}$. The R^2 value of the Langmuir model was

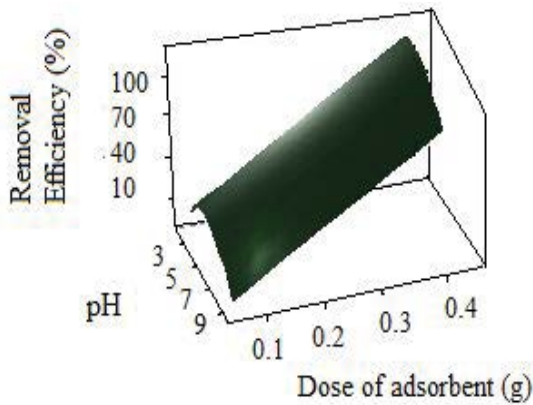


Fig. 10. Effect of dose of adsorbent, interaction of two variables (the amount of adsorbent (g) and pH), and their impact on removal efficiency of Pb(II) from aqueous solutions (Pb(II) concentration = 400 mg/L and contact time = 300 min).

0.99 and that of the Freundlich model was 0.96. Also, the *P* value of Langmuir and Freundlich model equaled 0.001 and 0.004, in that order. Therefore, the adsorption reaction of Pb²⁺ by CoFe₂O₄@CMC@HZSM-5 follows the Langmuir isotherm model. Accordingly, the Pb²⁺ adsorption using CoFe₂O₄@CMC@HZSM-5 is a type of monolayer adsorption. At the Langmuir adsorption isotherm, it is assumed that the adsorbed interacts with only a limited number of uniformly sites on adsorbent. In the Langmuir isotherm model, adsorption is limited to a single layer on the surface. Therefore, for all ions of a solution in the absorption process, there will be the same energy and enthalpy. $1/n$ is a heterogeneity parameter and n is the amount of deviation from the sorption line. If the value of n is equal to 1, the sorption process is a chemical process and if it is above 1, the sorption process is a physical process. Therefore, in this process, which n is less than 1, indicates that the sorption of lead on the CoFe₂O₄@CMC@HZSM-5 is a chemical process [69].

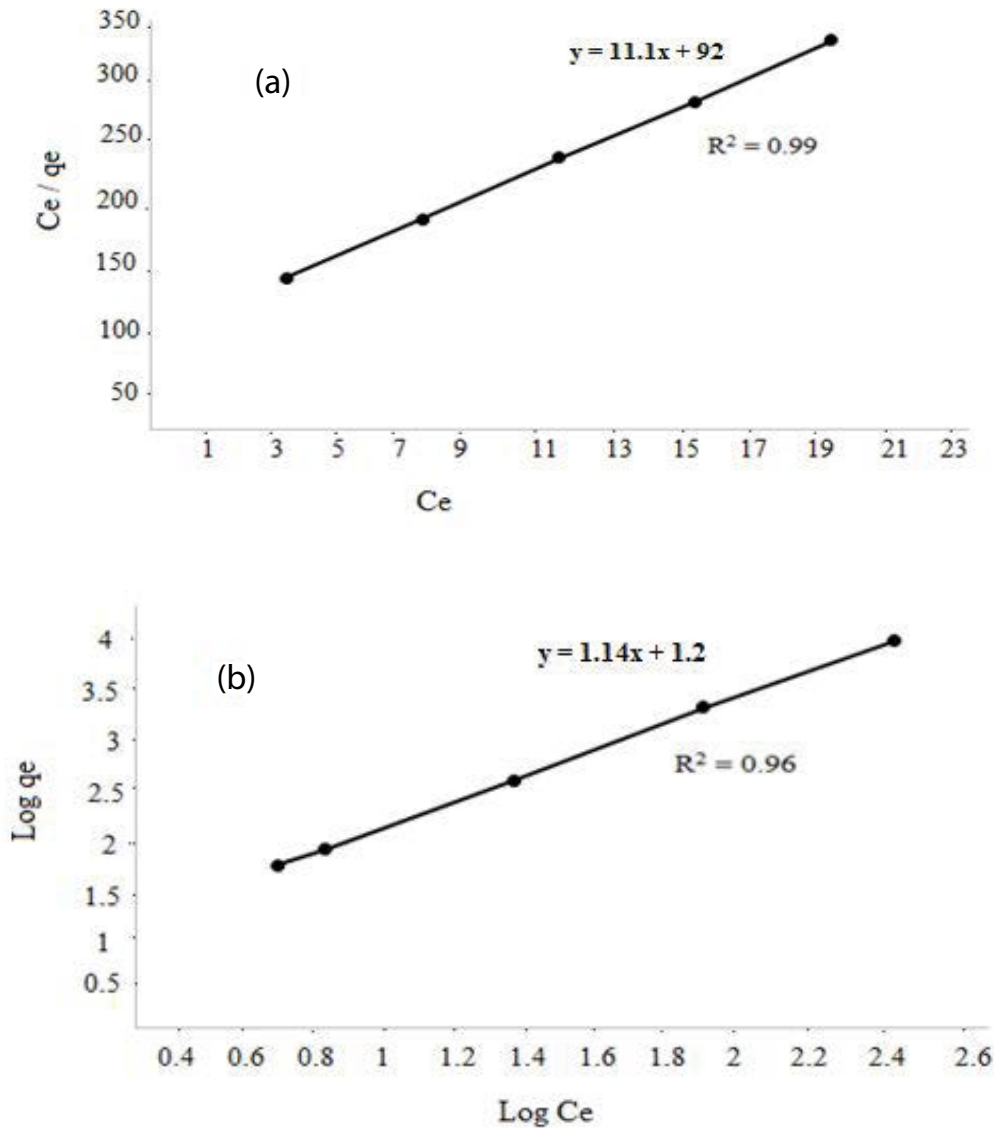


Fig. 11. Langmuir (a) and Freundlich isotherm (b) for adsorption of Pb(II) by CoFe₂O₄@CMC@HZSM-5.

3.7. Adsorption kinetics and thermodynamic study

The pseudo-first-order and pseudo-second-order models of Pb(II) on CoFe₂O₄@CMC@HZSM-5 are shown in Figs. 12a and b, respectively. The information about the adsorption kinetics of Pb(II) by CoFe₂O₄@CMC@HZSM-5 is given in Table 3. The R² of the pseudo-first- and pseudo-second-order models was 0.95 and 0.99, respectively. Moreover, the P-value of these models equaled 0.002 and 0.005, respectively. Accordingly, the adsorption reaction of Pb(II) using CoFe₂O₄@CMC@HZSM-5 is consistent

with the pseudo-second-order model that agrees with the Arancibia-Miranda et al. [5] and Shirzadi et al. [7] results. This proves the efficiency of adsorption at low Pb(II) concentrations [70,71]. Adsorption experiments were completed using synthetic solutions and at optimal conditions for real wastewater.

Table 4 shows the calculated thermodynamic data.

According to the negative ΔH° values, the removal of Pb(II) using CoFe₂O₄@CMC@HZSM-5 magnetic nano-biocomposite

Table 2
Parameters of the Langmuir and Freundlich adsorption isotherm models for adsorption of Pb(II) by CoFe₂O₄@CMC@HZSM-5

Langmuir			Freundlich		
Q ^s (mg/g)	b (L/mg)	R ²	K _f (mg/g)(L/mg)	n	R ²
142.8	0.03	0.99	2.02	0.5	0.96

Table 3
Adsorption kinetic coefficients of Pb(II) by CoFe₂O₄@CMC@HZSM-5

Pb(II) (mg/L)	Pseudo-second-order			Pseudo-first-order		
	R ²	k ₂	q _e	R ²	k ₁	q _e
50	0.99	0.03	91.2	0.95	0.1	83.22
200	0.99	0.04	72.14	0.95	0.11	81.86
400	0.99	0.06	56.63	0.95	0.12	87.92

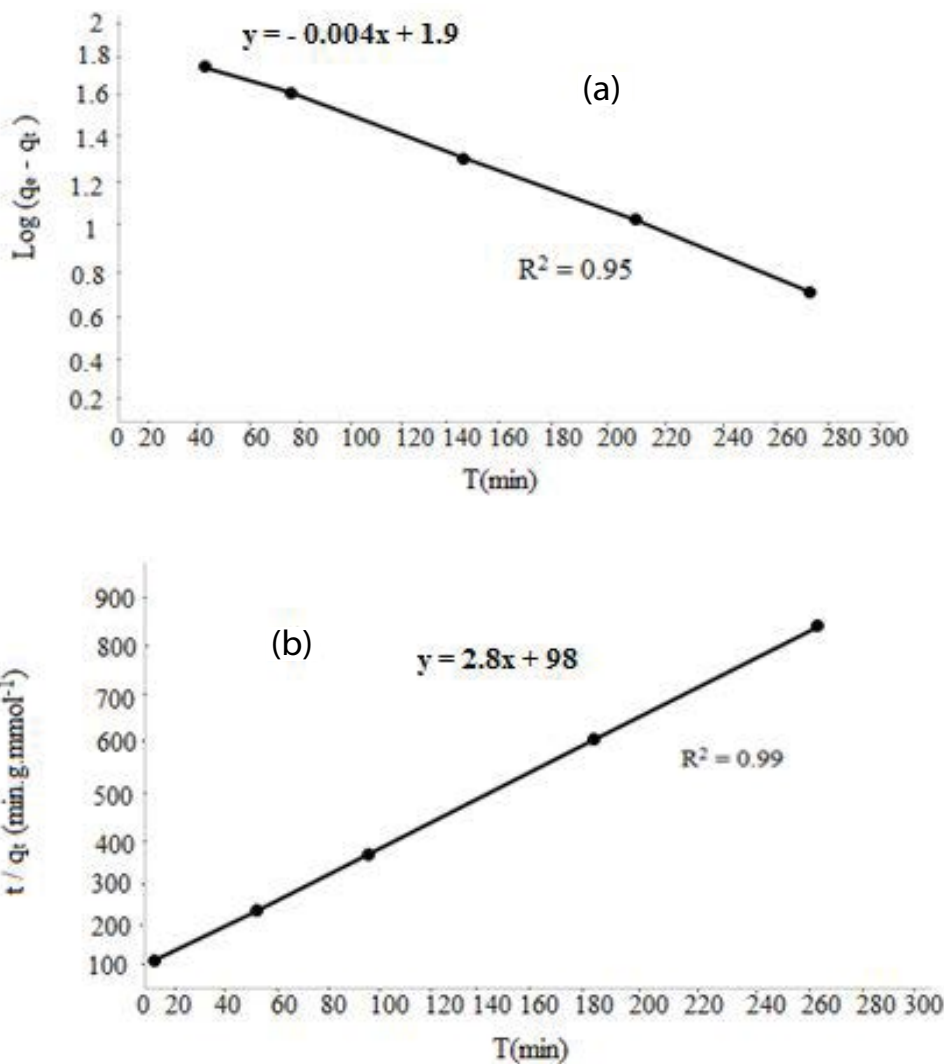


Fig. 12. Pseudo-first-order model (a) and pseudo-second-order model (b) of Pb(II) by CoFe₂O₄@CMC@HZSM-5.

Table 4
Thermodynamic parameters for Pb(II) sorption on CoFe₂O₄@CMC@HZSM-5

Temp. (K)	ΔG° (kJ/mol)	ΔH° (kJ/mol)	ΔS° (kJ/mol K)	K_c	C_e
288	10.7869			90.47	210
298	11.3101	-136.21	4.99	96.07	204
308	11.6120			93.2	207

is an exothermic process. As a result, according to Le Chatelier's principle, with increasing temperature, the progress of the reaction decreases and following that maximum absorption capacity is also reduced. Positive values of free energy indicate that the process in nature is not possible and spontaneous. These results are consistent with the findings of Zahedinia studies on the efficiency of *Populus nigra* sawdust in the removal of methylene blue from aqueous solutions [72].

3.8. Proposed sorption mechanism

CMC decreased the particle size of magnetic nanocomposite and increases the surface area of the nano-adsorbent. Additionally, the negative charge of carboxylate as functional groups of CMC causes electrostatic interaction between surface of the adsorbent and lead cations [73]. The adsorption mechanism is shown in Fig. 13.

Also, after the lead adsorption process, the adsorbent structure was investigated by EDS and mapping analyzes and the results are shown in Fig. 14. According to the results of EDS and mapping analyzes, it is observed that lead is adsorbed on the adsorbent surface.

3.9. Pb(II) removal from real wastewater

The highest removal efficiency and maximum adsorption capacity of Pb(II) using CoFe₂O₄@CMC@HZSM-5

with a 300-min contact time, pH = 5, Pb(II) concentration 400 mg/L, and the amount of adsorbent 0.4 g were 96% and 116.52 mg/g, respectively. The Pb(II) removal efficiency and adsorption capacity under optimal conditions for the real sample were reported as 75% and 90.32 mg/g, respectively. We chose the wastewater of a steel company as the real sample because it contained heavy metals. The quality of wastewater of the steel company containing lead is presented in Table 5. The removal efficiency in the real wastewater solution showed a decrease. The reduction in removal efficiency occurred by interference, such as the cations and anions available in the real wastewater.

Table 6 represents the removal efficiency of CoFe₂O₄@CMC@HZSM-5 for Pb(II) removal than that of other adsorbents.

This nanosorbent had a high efficiency in comparison with other mentioned adsorbents in less time, lower dose of adsorbent and higher concentration of Pb(II) and in real conditions it has shown high efficiency.

3.10. Regeneration and reusability of CoFe₂O₄@CMC@HZSM-5

The regeneration and reusability of the CoFe₂O₄@CMC@HZSM-5 magnetic nanoadsorbent were investigated for further evaluation of its possible use to treat Pb(II)-polluted water. Desorption test were carried out through ammonium acetate and disodium ethylenediamine tetraacetate (EDTA-2Na) as the eluents. The former is commonly

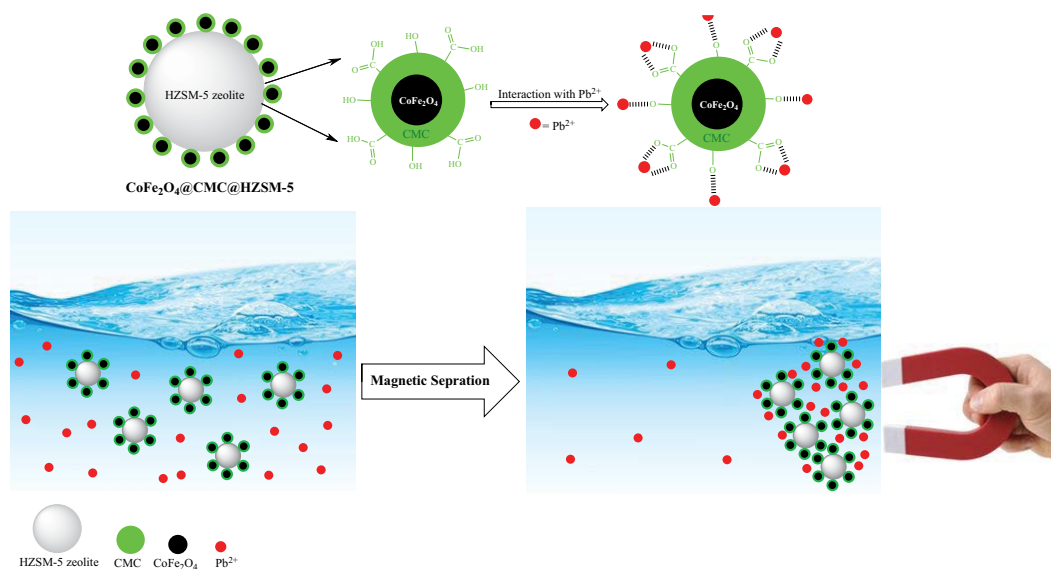


Fig. 13. Proposed mechanism of lead removal by CoFe₂O₄@CMC@HZSM-5.

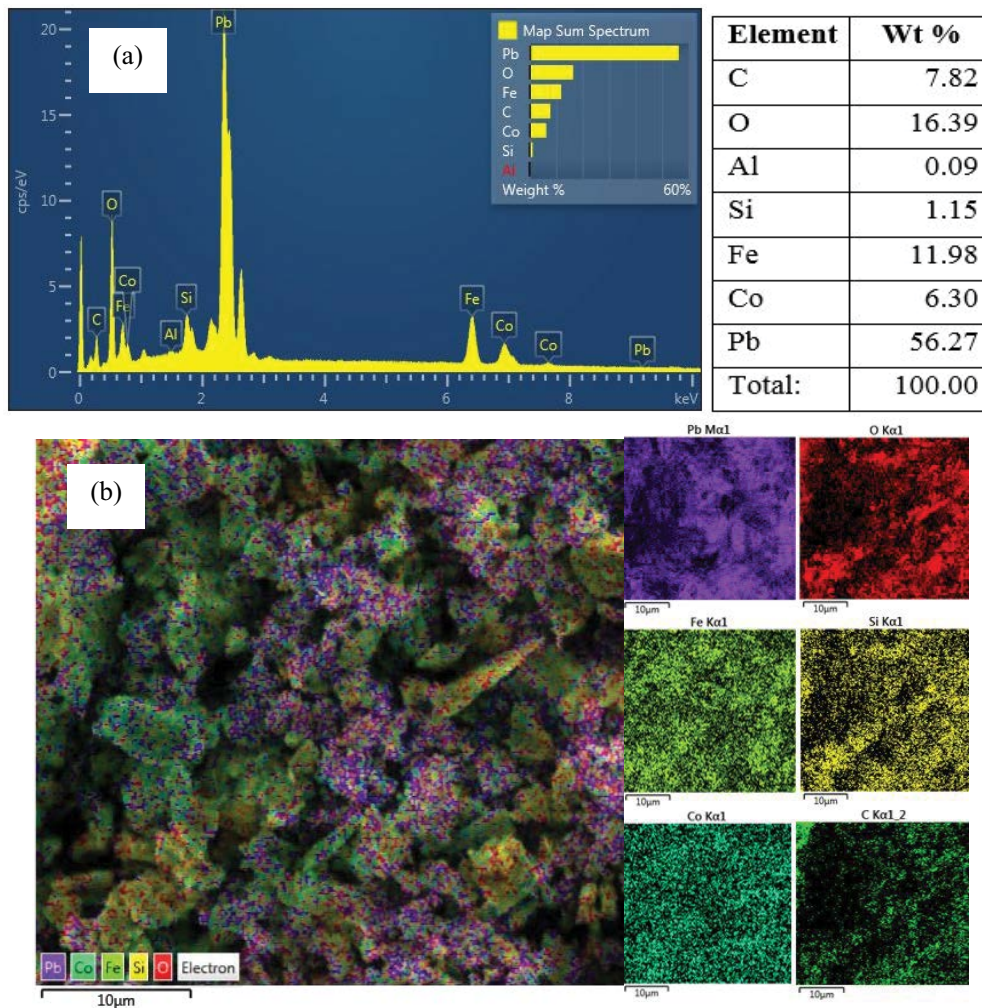


Fig. 14. The EDS (a) and mapping (b) of $\text{CoFe}_2\text{O}_4@\text{CMC}@\text{HZSM-5}$ magnetic nanoadsorbent after lead adsorption.

Table 5
Physicochemical properties of wastewater from steel company

Entry	Parameter	Amount
1	pH	7.4
2	EC (ds/m)	20.7
3	Turbidity (mg/L)	55
4	TSS (mg/L)	62
5	BOD (mg/L)	97
6	COD (mg/L)	50
7	SO_4^{2-} (mg/L)	15.68
8	NH_4^+ (mg/L)	3.7
9	VFC ($\mu\text{g/L}$)	481
10	Cu (mg/L)	0.06
11	Zn (mg/L)	0.12
12	Cd (mg/L)	0.33
13	Cr (mg/L)	0.1
14	Ni (mg/L)	0.038
15	Hg (mg/L)	0.41
16	Pb (mg/L)	0.02

used for measuring the cation exchange capacity (CEC) of clays due to its favorable ion-exchange capacity. The latter is commonly applied for eluting the metal ions captured by different adsorbents owing to its potent chelating capacity. Lead was desorbed from the surfaces of the $\text{CoFe}_2\text{O}_4@\text{CMC}@\text{HZSM-5}$ magnetic nanoadsorbent through soaking in 5×10^{-3} mol/L of the EDTA-2Na solution. Also, the same eluent was used for performing the regeneration test, and the recovered $\text{CoFe}_2\text{O}_4@\text{CMC}@\text{HZSM-5}$ was then reused for different sorption/desorption experiments. The lead removal efficiency slightly decreased from 96% to 91% after six successive cycles of adsorption–desorption experiments (Fig. 15). The small reduction in lead removal efficiency percentage can be caused by the slight loss of $\text{CoFe}_2\text{O}_4@\text{CMC}@\text{HZSM-5}$ concentration in the recovery process. However, our results indicated that the $\text{CoFe}_2\text{O}_4@\text{CMC}@\text{HZSM-5}$ magnetic nanoadsorbent exhibits a hopeful reproduction and recycling potential for the Pb(II) removal. In other words, this adsorbent material is able to support long-term use for the disposal of Pb(II)-bearing wastewater resulting in favorable cost performance.

Table 6

Comparison removal efficiency of $\text{CoFe}_2\text{O}_4\text{@CMC@HZSM-5}$ with various adsorbents to removal of Pb(II)

Entry	Adsorbents	Removal efficiency in synthetic solution (%)	Removal efficiency in real wastewater (%)	Adsorption capacity (mg/g)	References
1	Amino functionalized $\text{Fe}_3\text{O}_4\text{/NaP}$ zeolite nanocomposite	More than 95%	–	–	[74]
2	Nanoscale zero valent supported by zeolite and Montmorillonite	–	–	115.1	[7]
3	Magnetic zeolite NaA	Over 95%	–	–	[33]
4	Titanium oxide-bacterial cellulose bio-adsorbent	90%	–	–	[75]
5	Cobalt ferrite-supported activated carbon	96.4%	–	–	[76]
6	$\text{CoFe}_2\text{O}_4\text{@CMC@HZSM-5}$	96	75	116.52	This work

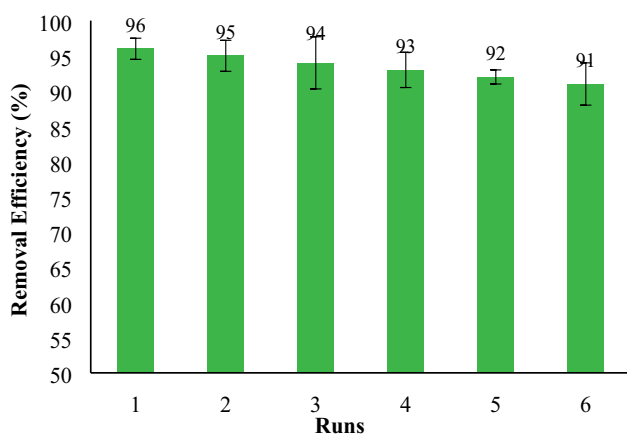


Fig. 15. Recycling of $\text{CoFe}_2\text{O}_4\text{@CMC@HZSM-5}$ magnetic nanoadsorbent in the EDTA-2Na as the eluent for removal of lead (Pb(II) concentration = 400 mg/L, contact time = 300 min, pH = 5 and amount of adsorbent = 0.4 g).

4. Conclusion

This study reported the synthesis of $\text{CoFe}_2\text{O}_4\text{@CMC@HZSM-5}$ as a novel magnetic nanoadsorbent to decontaminate Pb(II). Maximum removal efficiency Pb(II) by $\text{CoFe}_2\text{O}_4\text{@CMC@HZSM-5}$ magnetic nanoadsorbent in optimum conditions, including contact time of 300 min, pH of 5, level of 400 mg/L Pb(II), and an adsorbent amount of 0.4 g, was 96% for synthetic and 75% for real samples, respectively. The adsorption reaction of Pb(II) by $\text{CoFe}_2\text{O}_4\text{@CMC@HZSM-5}$ was in accordance with the Langmuir isotherm and pseudo-second-order kinetic models. Thermodynamics studies indicated that the adsorption of Pb(II) onto $\text{CoFe}_2\text{O}_4\text{@CMC@HZSM-5}$ was exothermic and was not possible and spontaneous in nature. Regarding its several effectiveness, including being environmental-friendly, cost-effectiveness, high stability and sorption capacity, satisfying reproduction performance, and easy magnetic separation characteristic, $\text{CoFe}_2\text{O}_4\text{@CMC@HZSM-5}$ can use as a potential adsorbent to treat polluted water including Pb(II) and heavy metals.

Acknowledgments

This research with project number 97000760 and IR.KMU.REC.1397.439 ethic approval cod was conducted in the Environmental Health Engineering Research Center of Kerman University of Medical Sciences.

Funding

This work was supported by the Vice-Chancellor for Research and Technology of Kerman University of Medical Sciences. The authors wish to thank the financial support of the Deputy of the Research Center at Said University.

References

- [1] Y. Wang, D. Yang, S. Li, M. Chen, L. Guo, J. Zhou, Ru/hierarchical HZSM-5 zeolite as efficient bi-functional adsorbent/catalyst for bulky aromatic VOCs elimination, *Microporous Mesoporous Mater.*, 258 (2018) 17–25.
- [2] J. Du, Y. Li, Z. Miao, Difunctional adsorbents Ni/ZnO-HZSM-5 on adsorption desulfurization and aromatization of olefin reaction, *Trans. Tianjin Univ.*, 25 (2019) 143–151.
- [3] H. Zhao, Sh. Jia, J. Cheng, X. Tang, M. Zhang, H. Yan, W. Ai, Experimental investigations of composite adsorbent 13X/CaCl₂ on an adsorption cooling system, *Appl. Sci.*, 7 (2017) 620, doi: 10.3390/app7060620.
- [4] S. Rajabi, A. Nasiri, M. Hashemi, Enhanced activation of persulfate by $\text{CuCoFe}_2\text{O}_4\text{@MC/AC}$ as a novel nanomagnetic heterogeneous catalyst with ultrasonic for metronidazole degradation, *Chemosphere*, 286 (2022) 131872, doi: 10.1016/j.chemosphere.2021.131872.
- [5] H. Shirzadi, A. Nezamzadeh-Ejehieh, An efficient modified zeolite for simultaneous removal of Pb(II) and Hg(II) from aqueous solution, *J. Mol. Liq.*, 230 (2017) 221–229.
- [6] I. Uogintė, G. Lujanienė, K. Mažeika, Study of Cu(II), Co(II), Ni(II) and Pb(II) removal from aqueous solutions using magnetic Prussian blue nano-sorbent, *J. Hazard. Mater.*, 369 (2019) 226–235.
- [7] N. Arancibia-Miranda, S.E. Baltazar, A. García, D. Muñoz-Lira, P. Sepúlveda, M.A. Rubio, D. Altbir, Nanoscale zero valent supported by zeolite and montmorillonite: template effect of the removal of lead ion from an aqueous solution, *J. Hazard. Mater.*, 301 (2016) 371–380.
- [8] M.K. Doula, A. Dimirkou, Use of an iron-overexchanged clinoptilolite for the removal of Cu²⁺ ions from heavily contaminated drinking water samples, *J. Hazard. Mater.*, 151 (2008) 738–745.

- [9] A. Takdastan, N. Mehrdadi, A. Torabian, A.A. Azimi, G.N. Bidhendi, Investigation of excess biological sludge reduction in sequencing batch reactor, *Asian J. Chem.*, 21 (2009) 2419–2427.
- [10] M. Ahmadi, S. Jarfi, A. Takdastan, N. Jafarzadeh, Study of efficiency of natural clinoptilolite zeolite in cadmium removal from aqueous solutions and determination of adsorption isotherms, *J. Ilam. Univ. Med. Sci.*, 23 (2015) 95–102.
- [11] S. Singh, K.C. Barick, D. Bahadur, Functional oxide nanomaterials and nanocomposites for the removal of heavy metals and dyes, *Nanotechnol.*, 3 (2013) 3–20.
- [12] M. Malakootian, H. Mahdizadeh, M. Khavari, A. Nasiri, M.A. Gharaghani, M. Khatami, E. Sahle-Demessie, R.S. Varma, Efficiency of novel Fe/charcoal/ultrasonic micro-electrolysis strategy in the removal of Acid Red 18 from aqueous solutions, *J. Environ. Chem. Eng.*, 8 (2020) 103553, doi: 10.1016/j.jece.2019.103553.
- [13] M. Malakootian, A. Nasiri, A.N. Alibeigi, H. Mahdizadeh, M.A. Gharaghani, Synthesis and stabilization of ZnO nanoparticles on a glass plate to study the removal efficiency of acid red 18 by hybrid advanced oxidation process (ultraviolet/ ZnO/ultrasonic), *Desal. Water Treat.*, 170 (2019) 325–336.
- [14] M. Malakootian, A. Nasiri, M. Khatami, H. Mahdizadeh, P. Karimi, M. Ahmadian, N. Asadzadeh, M.R. Heidari, Experimental data on the removal of phenol by electro- H_2O_2 in presence of UV with response surface methodology, *MethodsX*, 6 (2019) 1188–1193.
- [15] A. Nasiri, M. Malakootian, M.R. Heidari, S.N. Asadzadeh, $CoFe_2O_4$ @methylcellulose as a new magnetic nano biocomposite for sonocatalytic degradation of Reactive Blue 19, *J. Polym. Environ.*, 29 (2021) 2660–2675.
- [16] S. Rajabi, A. Nasiri, M. Hashemi, Enhanced activation of persulfate by $CuCoFe_2O_4$ @MC/AC as a novel nanomagnetic heterogeneous catalyst with ultrasonic for metronidazole degradation, *Chemosphere*, 286 (2022) 131872, doi: 10.1016/j.chemosphere.2021.131872.
- [17] A. Nasiri, F. Tamaddon, M.H. Mosslemine, M. Faraji, A microwave assisted method to synthesize nano $CoFe_2O_4$ @methyl cellulose as a novel metal-organic framework for antibiotic degradation, *MethodsX*, 6 (2019) 1557–1563.
- [18] A. Nasiri, F. Tamaddon, M.H. Mosslemine, M.A. Gharaghani, A. Asadipour, New magnetic nanobiocomposite $CoFe_2O_4$ @methylcellulose: facile synthesis, characterization, and photocatalytic degradation of metronidazole, *J. Mater. Sci. - Mater. Electron.*, 30 (2019) 8595–8610.
- [19] F. Tamaddon, A. Nasiri, G. Yazdanpanah, Photocatalytic degradation of ciprofloxacin using $CuFe_2O_4$ @methyl cellulose based magnetic nanobiocomposite, *MethodsX*, 7 (2020) 74–81.
- [20] S. Gunatilake, Methods of removing heavy metals from industrial wastewater, *Methods*, 1 (2015) 12–18.
- [21] M. Malakootian, Z. Darabi-Fard, N. Amirmahani, A. Nasiri, Evaluation of arsenic, copper, lead, cadmium, and iron concentration in drinking water resources of central and Southern Bardsir plain, Iran, in 2014, *J. Kerman Univ. Med. Sci.*, 22 (2015) 542–554 (in Persian).
- [22] M. Malakootian, M. Hashemi, A. Toolabi, A. Nasiri, Investigation of nickel removal using poly(amidoamine) generation 4 dendrimer (PAMAM G4) from aqueous solutions, *J. Eng. Res. (Kuwait)*, 6 (2018) 13–23.
- [23] N. Javid, A. Nasiri, M. Malakootian, Removal of nonylphenol from aqueous solutions using carbonized date pits modified with ZnO nanoparticles, *Desal. Water Treat.*, 141 (2019) 140–148.
- [24] A. Nasiri, M. Malakootian, M.A. Shiri, G. Yazdanpanah, M. Nozari, $CoFe_2O_4$ @methylcellulose synthesized as a new magnetic nanocomposite to tetracycline adsorption: modeling, analysis, and optimization by response surface methodology, *J. Polym. Res.*, 28 (2021), doi: 10.1007/s10965-021-02540-y.
- [25] M. Malakootian, A. Nasiri, H. Mahdizadeh, Metronidazole adsorption on $CoFe_2O_4$ /activated carbon@chitosan as a new magnetic biocomposite: modelling, analysis, and optimization by response surface methodology, *Desal. Water Treat.*, 164 (2019) 215–227.
- [26] A. Gaffer, A.A. Al Kahlawy, D. Aman, Magnetic zeolite-natural polymer composite for adsorption of chromium(VI), *Egypt. J. Pet.*, 26 (2017) 995–999.
- [27] O. Eljamal, T. Shubair, A. Tahara, Y. Sugihara, N. Matsunaga, Iron based nanoparticles-zeolite composites for the removal of cesium from aqueous solutions, *J. Mol. Liq.*, 277 (2019) 613–623.
- [28] A. Loiola, J. Andrade, J. Sasaki, L. Da Silva, Structural analysis of zeolite NaA synthesized by a cost-effective hydrothermal method using kaolin and its use as water softener, *J. Colloid Interface Sci.*, 367 (2012) 34–39.
- [29] D.W. Breck, Z.M. Sieves, Structure, Chemistry and Use, *Zeolite Molecular Sieves*, Wiley, New York, 1974.
- [30] H. Liu, S. Peng, L. Shu, T. Chen, T. Bao, R.L. Frost, Magnetic zeolite NaA: synthesis, characterization based on metakaolin and its application for the removal of Cu^{2+} , Pb^{2+} , *Chemosphere*, 91 (2013) 1539–1546.
- [31] G.M. Haggerty, R.S. Bowman, Sorption of chromate and other inorganic anions by organo-zeolite, *Environ. Sci. Technol.*, 28 (1994) 452–458.
- [32] E. Sullivan, J. Carey, R. Bowman, Thermodynamics of cationic surfactant sorption onto natural clinoptilolite, *J. Colloid Interface Sci.*, 206 (1998) 369–380.
- [33] Y. Zeng, H. Woo, G. Lee, J. Park, Adsorption of Cr(VI) on hexadecylpyridinium bromide (HDPB) modified natural zeolites, *Microporous Mesoporous Mater.*, 130 (2010) 83–91.
- [34] H. Faghihian, R.S. Bowman, Adsorption of chromate by clinoptilolite exchanged with various metal cations, *Water Res.*, 39 (2005) 1099–1104.
- [35] P. Ambrozova, J. Kynicky, T. Urubek, V.D. Nguyen, Synthesis and modification of clinoptilolite, *Molecules*, 22 (2017) 1107, doi: 10.3390/molecules22071107.
- [36] K. Murakami, T. Wajima, T. Kato, K. Sugawara, T. Sugawara, Thermodynamic and kinetic studies on Cs^+ - and Sr^{2+} -exchange in natural zeolite from Akita, Japan, *Toxicol. Environ. Chem.*, 91 (2009) 1023–1034.
- [37] H. Faghihian, M. Moayed, A. Firooz, M. Irvani, Synthesis of a novel magnetic zeolite nanocomposite for removal of Cs^+ and Sr^{2+} from aqueous solution: kinetic, equilibrium, and thermodynamic studies, *J. Colloid Interface Sci.*, 393 (2013) 445–451.
- [38] L.R. Rad, A. Momeni, B.F. Ghazani, M. Irani, M. Mahmoudi, B. Noghreh, Removal of Ni^{2+} and Cd^{2+} ions from aqueous solutions using electrospun PVA/zeolite nanofibrous adsorbent, *Chem. Eng. J.*, 256 (2014) 119–127.
- [39] R.I. Yousef, B. El-Eswed, H. Ala'a, Adsorption characteristics of natural zeolites as solid adsorbents for phenol removal from aqueous solutions: kinetics, mechanism, and thermodynamics studies, *Chem. Eng. J.*, 171 (2011) 1143–1149.
- [40] H. RunPing, Z. Lina, Z. Xin, X. YanFang, X. Feng, L. YinLi, W. Yu, Characterization and properties of iron oxide-coated zeolite as adsorbent for removal of copper(II) from solution in fixed bed column, *Chem. Eng. J.*, 149 (2009) 123–131.
- [41] J. Bauer, R. Herrmann, W. Mittelbach, W. Schwieger, Zeolite/aluminum composite adsorbents for application in adsorption refrigeration, *Int. J. Energy Res.*, 33 (2009) 1233–1249.
- [42] O. Falyouna, O. Eljamal, I. Maamoun, A. Tahara, Y. Sugihara, Magnetic zeolite synthesis for efficient removal of cesium in a lab-scale continuous treatment system, *J. Colloid Interface Sci.*, 571 (2020) 66–79.
- [43] Z. Zhao, X. Cui, J. Ma, R. Li, Adsorption of carbon dioxide on alkali-modified zeolite 13X adsorbents, *Int. J. Greenhouse Gas Control*, 1 (2007) 355–359.
- [44] R. Han, W. Zou, H. Li, Y. Li, J. Shi, Copper(II) and lead(II) removal from aqueous solution in fixed-bed columns by manganese oxide coated zeolite, *J. Hazard. Mater.*, 137 (2006) 934–942.
- [45] L.C. Oliveira, D.I. Petkowicz, A. Smianotto, S.B. Pergher, Magnetic zeolites: a new adsorbent for removal of metallic contaminants from water, *Water Res.*, 38 (2004) 3699–3704.
- [46] A. Takahashi, R.T. Yang, C.L. Munson, D. Chinn, Cu(I)-Y-zeolite as a superior adsorbent for diene/olefin separation, *Langmuir*, 17 (2001) 8405–8413.

- [47] B. Huang, M. Lu, D. Wang, Y. Song, L. Zhou, Versatile magnetic gel from peach gum polysaccharide for efficient adsorption of Pb^{2+} and Cd^{2+} ions and catalysis, *Carbohydr. Polym.*, 181 (2018) 785–792.
- [48] S. Ashyüce, N. Bereli, A. Topçu, P.W. Ranteke, A. Denizli, Indian saffron – turmeric (*Curcuma longa*) embedded supermacroporous cryogel discs for heavy metal removal, *Biointerface Res. Appl. Chem.*, 9 (2019) 4356–4361.
- [49] J. Ifthikar, J. Wang, Q. Wang, T. Wang, H. Wang, A. Khan, A. Jawad, T. Sun, X. Jiao, Z. Chen, Highly efficient lead distribution by magnetic sewage sludge biochar: sorption mechanisms and bench applications, *Bioresour. Technol.*, 238 (2017) 399–406.
- [50] H. Wang, Y. Liu, J. Ifthikar, L. Shi, A. Khan, Z. Chen, Z. Chen, Towards a better understanding on mercury adsorption by magnetic bio-adsorbents with $\gamma\text{-Fe}_2\text{O}_3$ from pinewood sawdust derived hydrochar: influence of atmosphere in heat treatment, *Bioresour. Technol.*, 256 (2018) 269–276.
- [51] J. Ifthikar, X. Jiao, A. Ngambia, T. Wang, A. Khan, A. Jawad, Q. Xue, L. Lui, Z. Chen, Facile one-pot synthesis of sustainable carboxymethyl chitosan – sewage sludge biochar for effective heavy metal chelation and regeneration, *Bioresour. Technol.*, 262 (2018) 22–31.
- [52] H. Wang, S. Wang, Z. Chen, X. Zhou, J. Wang, Z. Chen, Engineered biochar with anisotropic layered double hydroxide nanosheets to simultaneously and efficiently capture Pb^{2+} and CrO_4^{2-} from electroplating wastewater, *Bioresour. Technol.*, 306 (2020) 123118, doi: 10.1016/j.biortech.2020.123118.
- [53] H. Wang, J. Cai, Z. Liao, A. Jawad, J. Ifthikar, Z. Chen, Z. Chen, Black liquor as biomass feedstock to prepare zero-valent iron embedded biochar with red mud for $Cr(VI)$ removal: mechanisms insights and engineering practicality, *Bioresour. Technol.*, 311 (2020) 123553, doi: 10.1016/j.biortech.2020.123553.
- [54] G.G. Aregay, A. Jawad, Y. Du, A. Shahzad, Z. Chen, Efficient and selective removal of chromium(VI) by sulfide assembled hydrotalcite compounds through concurrent reduction and adsorption processes, *J. Mol. Liq.*, 294 (2019) 111532, doi: 10.1016/j.molliq.2019.111532.
- [55] T. Kamal, Y. Anwar, Sh. Bahadar Khan, M. Tariq Saeed Chani, A.M. Asiri, Dye adsorption and bactericidal properties of TiO_2 /chitosan coating layer, *Carbohydr. Polym.*, 148 (2016) 153–160.
- [56] T. Kamal, M. Ul-Islam, Sh. Bahadar Khan, A.M. Asiri, Adsorption and photocatalyst assisted dye removal and bactericidal performance of ZnO /chitosan coating layer, *Int. J. Biol. Macromol.*, 81 (2018) 584–590.
- [57] Sh. Bahadar Khan, F. Ali, T. Kamal, Y. Anwar, A.M. Asiri, J. Seo, CuO embedded chitosan spheres as antibacterial adsorbent for dyes, *Int. J. Biol. Macromol.*, 88 (2016) 113–119.
- [58] Sh. Ali Khan, Sh. Bahadar Khan, T. Kamal, M. Yasir, A.M. Asiri, Antibacterial nanocomposites based on chitosan/Co-MCM as a selective and efficient adsorbent for organic dyes, *Int. J. Biol. Macromol.*, 91 (2016) 744–751.
- [59] I. Ahmad, Sh. Bahadar Khan, T. Kamal, A.M. Asiri, Visible light activated degradation of organic pollutants using zinc-iron selenide, *J. Mol. Liq.*, 229 (2017) 429–435.
- [60] Sh. Bahadar Khan, Sh. Ali Khan, H.M. Marwani, E.M. Bakhsh, Y. Anwar, T. Kamal, A.M. Asiri, K. Akhtar, Anti-bacterial PES-cellulose composite spheres: dual character toward extraction and catalytic reduction of nitrophenol, *RSC Adv.*, 6 (2016) 110077–110090.
- [61] T. Benhalima, H. Ferfera-Harrar, Eco-friendly porous carboxymethyl cellulose/dextran sulfate composite beads as reusable and efficient adsorbents of cationic dye methylene blue, *Int. J. Biol. Macromol.*, 132 (2019) 126–141.
- [62] M. Malakootian, A. Nasiri, H. Mahdizadeh, Preparation of $CoFe_2O_4$ /activated carbon@chitosan as a new magnetic nanobiocomposite for adsorption of ciprofloxacin in aqueous solutions, *J. Water Sci. Technol.*, 78 (2018) 2158–2170.
- [63] F. Aeenjan, V. Javanbakht, Methylene blue removal from aqueous solution by magnetic clinoptilolite/chitosan/EDTA nanocomposite, *Res. Chem. Intermed.*, 44 (2018) 1459–1483.
- [64] S. Kim, T.G. Lee, Removal of $Cr(VI)$ from aqueous solution using functionalized poly(GMA-co-EGDMA)-graft-poly(allylamine), *React. Funct. Polym.*, 134 (2019) 133–140.
- [65] I. Maamoun, O. Eljamal, O. Falyouna, R. Eljamal, Y. Sugihara, Multi-objective optimization of permeable reactive barrier design for $Cr(VI)$ removal from groundwater, *Ecotoxicol. Environ. Saf.*, 200 (2020) 110773, doi: 10.1016/j.ecoenv.2020.110773.
- [66] H. Faghilian, M. Moayed, A. Firooz, M. Irvani, Synthesis of a novel magnetic zeolite nanocomposite for removal of Cs^+ and Sr^{2+} from aqueous solution: kinetic, equilibrium, and thermodynamic studies, *J. Colloid Interface Sci.*, 393 (2013) 445–451.
- [67] F. Veisi, A. Veisi, Modeling bisphenol A removal from aqueous solution by activated carbon and eggshell, *J. Mazandaran Univ. Med. Sci.*, 22 (2013) 129–138.
- [68] S. Venkateswarlu, B.N. Kumar, B. Prathima, Y. SubbaRao, N.V.V. Jyothi, A novel green synthesis of Fe_3O_4 magnetic nanorods using *Punica Granatum* rind extract and its application for removal of $Pb(II)$ from aqueous environment, *Arabian J. Chem.*, 12 (2019) 588–596.
- [69] I. Maamoun, O. Eljamal, R. Eljamal, O. Falyouna, Y. Sugihara, Promoting aqueous and transport characteristics of highly reactive nanoscale zero valent iron via different layered hydroxide coatings, *Appl. Surf. Sci.*, 506 (2020) 145018, doi: 10.1016/j.apsusc.2019.145018.
- [70] I. Maamoun, O. Eljamal, O. Falyouna, R. Eljamal, Y. Sugihara, Stimulating effect of magnesium hydroxide on aqueous characteristics of iron nanocomposites, *Water Sci. Technol.*, 80 (2019) 1996–2002.
- [71] J.H. Cheong, K.J. Lee, Removal of Co^{2+} ions from aqueous solution by ferrite process, *Sep. Sci. Technol.*, 31 (1996) 1137–1160.
- [72] E.A. Mehrizi, M. Sadani, M. Karimaei, E. Ghahramani, K. Ghadiri, M.S. Taghizadeh, Isotherms and kinetics of lead and cadmium uptake from the waste leachate by natural adsorbent, *World Appl. Sci. J.*, 15 (2011) 1678–1686.
- [73] R. Eljamal, O. Eljamal, I. Maamoun, G. Yilmaz, Y. Sugihara, Enhancing the characteristics and reactivity of nZVI: polymers effect and mechanisms, *J. Mol. Liq.*, 315 (2020) 113714, doi: 10.1016/j.molliq.2020.113714.
- [74] M. Zendehtdel, M. Ramezani, B. Shoshtari-Yeganeh, G. Cruciani, A. Salmani, Simultaneous removal of $Pb(II)$, $Cd(II)$ and bacteria from aqueous solution using amino-functionalized Fe_3O_4/NaP zeolite nanocomposite, *Environ. Technol.*, 40 (2019) 3689–3704.
- [75] A. Shoukat, F. Wahid, T. Khan, M. Siddique, S. Nasreen, G. Yang, M. Wajid Ullah, R. Khan, Titanium oxide-bacterial cellulose bioadsorbent for the removal of lead ions from aqueous solution, *Int. J. Biol. Macromol.*, 129 (2019) 965–971.
- [76] M. Yahya, K. Obayomi, M. Abdulkadir, Y. Iyaka, A. Olugbenga, Characterization of cobalt ferrite-supported activated carbon for removal of chromium and lead ions from tannery wastewater via adsorption equilibrium, *Water Sci. Eng.*, 13 (2020) 202–213.